J Mater Sci (2017) 52:8258–8267

Lightweight ferroferric oxide nanotubes with natural resonance property and design for broadband microwave absorption

Peng He[1], Zhi-Ling Hou[1,*], Kai-Lun Zhang[1], Jun Li[2], Kai Yin[1], Shuo Feng[1], and Song Bi[2,*]

[1] School of Science and Beijing Key Laboratory of Environmentally Harmful Chemicals Assessment, Beijing University of Chemical Technology, Beijing 100029, People's Republic of China
[2] 501 Department, Xi'an Research Institute of High-Tech, Xi'an 710025, People's Republic of China

Received: 10 January 2017
Accepted: 24 March 2017
Published online: 31 March 2017

ABSTRACT

Due to strong magnetism along with low density and low percolation threshold, hollow Fe_3O_4 nanostructures have important potential applications in absorbing materials. In this work, Fe_3O_4 nanotubes with both dielectric and magnetic losses, namely bi-loss features, were obtained through two-step chemical methods (hydrothermal method and activated carbon reduction). The Fe_3O_4 nanotubes show high dielectric loss due to the electronic relaxation polarization, and the concentration dependence of dielectric properties for Fe_3O_4 nanotubes composite can be well described by the effective dielectric theory. In comparison with bulk Fe_3O_4 with natural ferromagnetic resonance around 1.2 GHz, the as-prepared Fe_3O_4 nanotubes present a natural resonant peak at 4 GHz frequency, leading to the higher magnetic loss in the radar band (2–18 GHz). Therefore, the Fe_3O_4 nanotubes show better microwave absorption with minimum reflection loss up to −50.94 dB compared with other Fe_3O_4 nanostructures. Moreover, double loss peaks were observed in 70 and 80 wt% samples with thickness of 5 mm, making this material a good candidate for designing broadband metastructure absorber.

Introduction

Microwave absorption materials have attracted tremendous attention [1–6] owing to their military and civil application such as converting electromagnetic energy into heat, microwave darkrooms and microwave interference protection [7]. Possessing aligned magnetic dipoles under electromagnetic fields [8], magnetic [9] and multiferrite materials [10] coupled with failure mechanisms are not only critical in the investigation of electromagnetic and mechanical–magnetic response materials and devices [11–16], but also greatly contribute to microwave absorption applications [17–23] due to the fact that it is easy to fabricate thinner absorbers than non-magnetic materials. In addition, ferrites can avoid the skin effect at high frequency owing to their high

Address correspondence to E-mail: houzl@mail.buct.edu.cn; bisong5011@163.com

DOI 10.1007/s10853-017-1041-6

resistivity. Therefore, electromagnetic wave can be attenuated efficiently. Recently, there been a growing and widespread interest in nanostructured magnetite (Fe_3O_4) as a potential microwave absorbing materials due to its higher dielectric and magnetic loss. For example, Liu et al. [24] prepared elliptical Fe_3O_4 nanorings, which exhibited significantly enhanced microwave absorption performance compared with Fe_3O_4 circular nanorings. Wen et al. [25] reported that Fe_3O_4 nanoparticles with smaller size presented better microwave absorbing properties. Sun et al. [22] prepared Fe_3O_4 dendritic microstructures, which presented better microwave absorbing properties than nanospheres. Therefore, size and nanostructure play an important role in the microwave absorption. Compared with traditional absorption materials, nanotube structure has lower percolation threshold and lower density, which is a great help to improve microwave absorption. For example, Zhu et al. [26] reported that the $BaTiO_3$ nanotubes composite showed a minimum reflection loss of −21.8 dB at 15 GHz, and the frequency bandwidth less than −10 dB is from 13.3 to 15 GHz. Qi et al. [27] reported that a minimum reflection loss of −32.7 dB is observed at 4.6 GHz for the carbon nanotube (CNT) composite. Wang et al. [28] reported that Co–Ni–P nanotubes exhibited the lowest reflection loss of −57.8 at 16.45 GHz. Owing to strong magnetism, low percolation threshold and low density, Fe_3O_4 nanotube may be a kind of good potential candidate for microwave absorbing materials.

In this paper, Fe_3O_4 nanotubes were synthesized through two-step chemical methods. First, α-Fe_2O_3 nanotubes were got by the hydrothermal method. Then, Fe_3O_4 nanotubes were obtained by the activated carbon reduction in α-Fe_2O_3 nanotubes. We investigated the complex permittivity, complex permeability and microwave absorption properties of Fe_3O_4 nanotubes in the range of 0.5–18 GHz. As expected, Fe_3O_4 nanotubes show an excellent microwave absorption property and the corresponding mechanisms were further discussed.

Materials and methods

Synthesis of Fe_3O_4 nanotubes

All the solvents and chemicals were of analytical grade and used without further purification. Fe_3O_4 nanotubes were prepared by two-step chemical methods. First, 1.6×10^{-3} mol $FeCl_3{\cdot}6H_2O$ and 6.4×10^{-5} mol $NaH_2PO_4{\cdot}2H_2O$ were first mixed by 70 mL deionized water and then dispersed uniformly by ultrasonication for 15 min. The mixed solution was sealed in a 100-mL Teflon-lined stainless steel autoclave and hydrothermally treated for 24 h at 240 °C. A red precipitate was obtained at the bottom of the autoclave and was separated by centrifugation. The precipitate was washed three times with ethyl alcohol and distilled water and then dried at 70 °C in air. The resulting powder was α-Fe_2O_3 nanotube. Second, the synthesized α-Fe_2O_3 nanotubes were mixed with activated carbon and heat-treated in a tubular oven under N_2 at 480 °C for 3 h. A black powder was obtained. The resulting black powder was a mixture of activated carbon and Fe_3O_4 nanotubes. Then, Fe_3O_4 nanotubes were separated by magnet and washed three times with ethyl alcohol and distilled water. At last, pure Fe_3O_4 nanotubes were obtained, and the process is shown in Fig. 1.

Characterization

The initial investigation of structural and microstructure analysis was carried out by the X-ray diffractometer (XRD) using Cu Kα radiation with wave length 1.54 Å and scanning electron microscope (SEM). The magnetic properties were achieved by a physical property measurement system (Quantum Design Inc.). The electromagnetic parameters of the sample were measured by a vector network analyzer system (E5071C) in the range 0.5–18 GHz. The composite samples for electromagnetic parameter measurements were prepared by evenly mixing the product with a paraffin wax in mass ratio of 1:1, 3:2, 7:3, 4:1 [29], and then being pressed into a mold with an outer diameter of 7 mm, inner diameter of 3 mm and thickness of about 2 mm. The electrical conductivity was measured by a digit multimeter (34401A). The microwave absorbing properties of Fe_3O_4 nanotubes metastructure investigated in simulation through commercial software CST studio suite 2014 by the electromagnetic properties of the sample with 80 wt%.

Results and discussion

Microstructure and phase analysis

Figure 2 shows the XRD pattern of as-synthesized samples. The top shows α-Fe_2O_3 phase (hematite, JCPDS No. 24-0072), which has a rhombohedral structure with the lattice parameters of the a = 5.0320

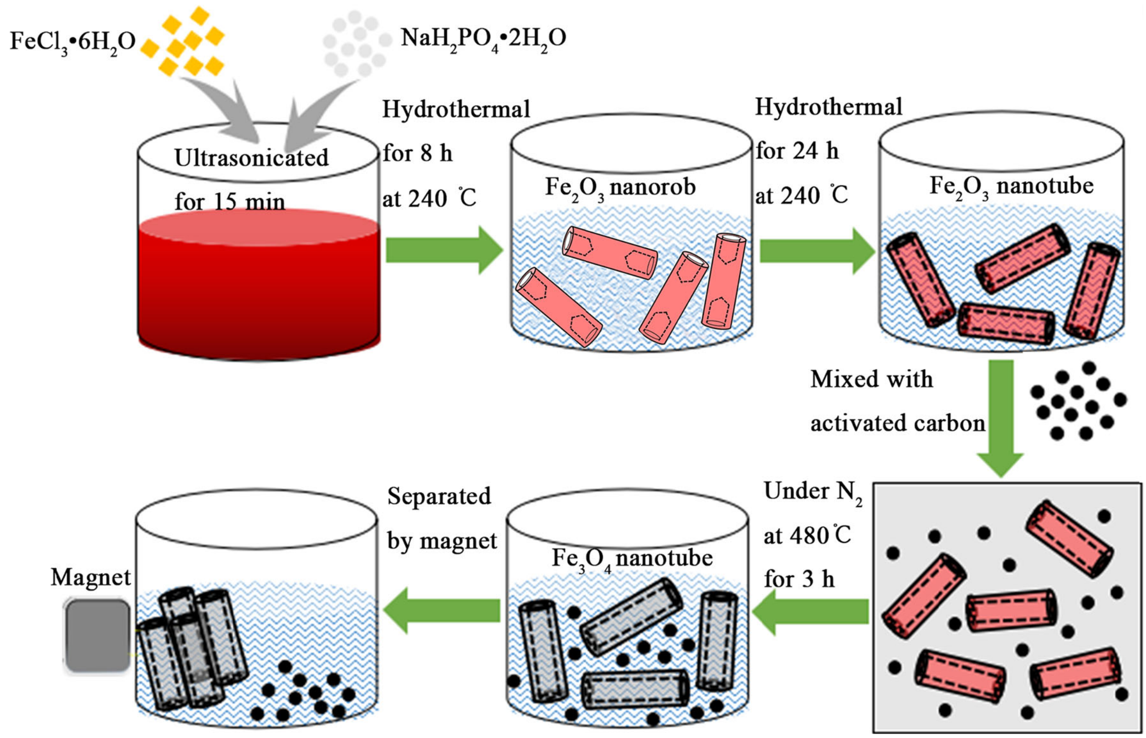

Figure 1 Schematic diagram of producing Fe_3O_4 nanotubes.

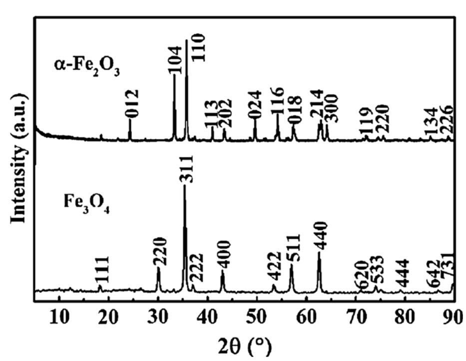

Figure 2 XRD pattern of the typical as-synthesized samples.

and $c = 13.7619$ Å. As shown in the bottom of Fig. 2, all the peaks can be indexed as face-centered cubic Fe_3O_4 with space group of F*d*-3 m and lattice constant $a = 8.387$ Å, which is in good agreement with JCPDS, No. 89-0691. No impurity phases can be observed in Fe_3O_4 nanotubes.

Figure 3 shows SEM images of α-Fe_2O_3 nanotubes and Fe_3O_4 nanotubes. Fe_3O_4 holds the same nanostructure and size as α-Fe_2O_3. The length of nanotube is about 200–400 nm, and all the tubes contain through-holes with diameter about 50–80 nm. Besides, the ratio of length to diameter is about 2.5–8.

Magnetic properties

The Fe_3O_4 nanotubes can be quickly separated from a dispersion of them by an external magnetic field as shown in Fig. 4a, suggesting that Fe_3O_4 nanotubes possess strong magnetism. Figure 4b shows the *M*–*H* loops of the Fe_3O_4 nanotubes at room temperature, with the fields weeping from −20000 to 20000 Oe. The saturation magnetization (M_s), remanent magnetization (M_r) and coercivity (H_c) are 63.3, 13.25 emu/g and 249.62 Oe, respectively. M_s value for Fe_3O_4 nanotubes are lower than those for corresponding bulk Fe_3O_4 ($M_r = 92$ emu/g), which is caused by the spin disorder on the surface and surface oxidation [22]. However, the H_c of Fe_3O_4 nanotubes are obviously higher than that of corresponding bulk Fe_3O_4 ($H_c = 115$–150 Oe), which is due to the absence of the vortex states and the presence of out-plane and in-plane spin configurations [30].

Electromagnetic properties and microwave absorbing properties

Figure 5a, b shows the real and imaginary parts of the complex relative permittivity (ε', ε''). With

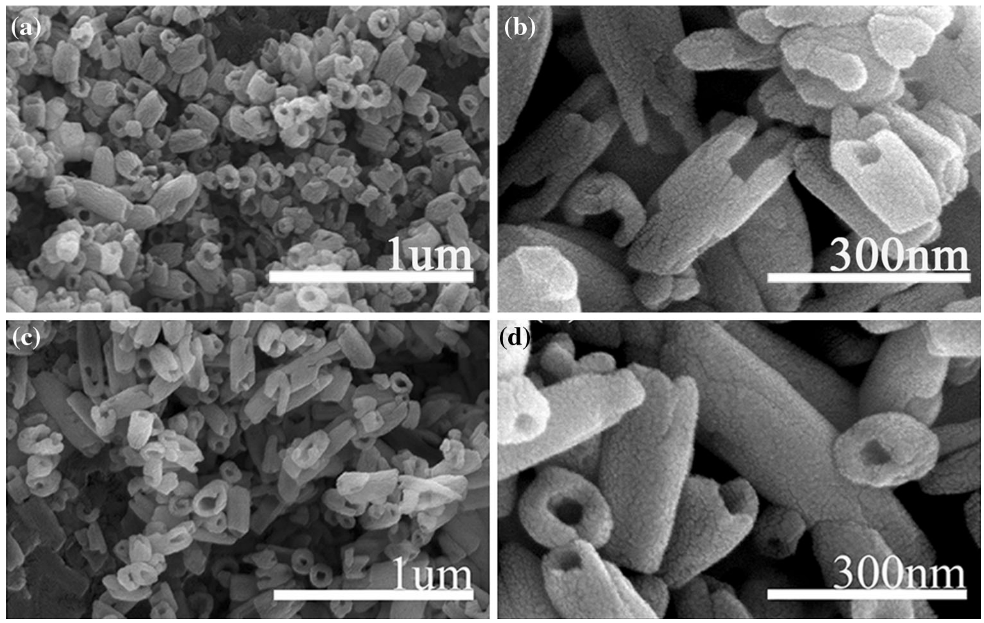

Figure 3 Low (**a**, **c**), high (**b**, **d**) magnification SEM images of α-Fe_2O_3 and Fe_3O_4 nanotubes.

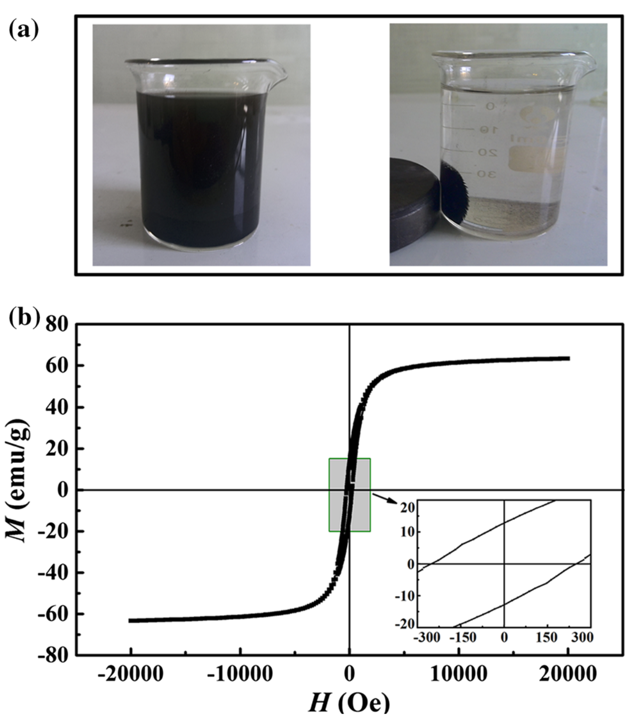

Figure 4 **a** The picture of the Fe_3O_4 nanotubes quickly separated from a dispersion of them by an external magnetic field. **b** Hysteresis loop of the Fe_3O_4 nanotube. The *inset* shows the magnified plot.

increasing frequency, the ε' of each sample slightly decreased, showing the behavior of Debye relaxation. However, the ε' increases along with increased Fe_3O_4 nanotubes weight fraction and ε'' also shows the same trend. There is a little difference in ε'' between 50 and 60 wt%, which may be caused by the low concentration of two samples and instrumental error. In fact, Fe_3O_4 has good electrical conductivity due to transfer of electrons between Fe^{2+} and Fe^{3+} in the octahedral sites as shown in the inset of Fig. 5c. In order to determine whether this dielectric loss is dominated by direct current electric conductance loss (ε_D''), direct current electrical conductivity (γ) was measured. The relationship of ε'' and ε_D'' can be expressed by

$$\varepsilon'' = \varepsilon_D'' + \varepsilon_R'' \tag{1}$$

here $\varepsilon_D'' = \frac{\gamma}{2\pi f \varepsilon_0}$, where f is the frequency, ε_0 is the dielectric constant of vacuum, and ε_R'' is electronic relaxation loss. Figure 5c shows the frequency dependence of ε_D'' for Fe_3O_4 nanotubes composite with 70 and 80 wt%. However, the γ with 50 and 60 wt% is too small to be measured. Obviously, ε_D'' for two samples is much smaller than ε'' for two samples, and it indicates that the dielectric loss is dominated by electronic relaxation loss. Schematic diagram of dielectric loss mechanism is shown in Fig. 5d. Electron hoping between two adjacent nanotubes under applied electric field leads to electrical conduction, but the potential barrier of transition is high; then, ε_D'' is too small. The potential barrier of transition is higher when the distance between two nanotubes

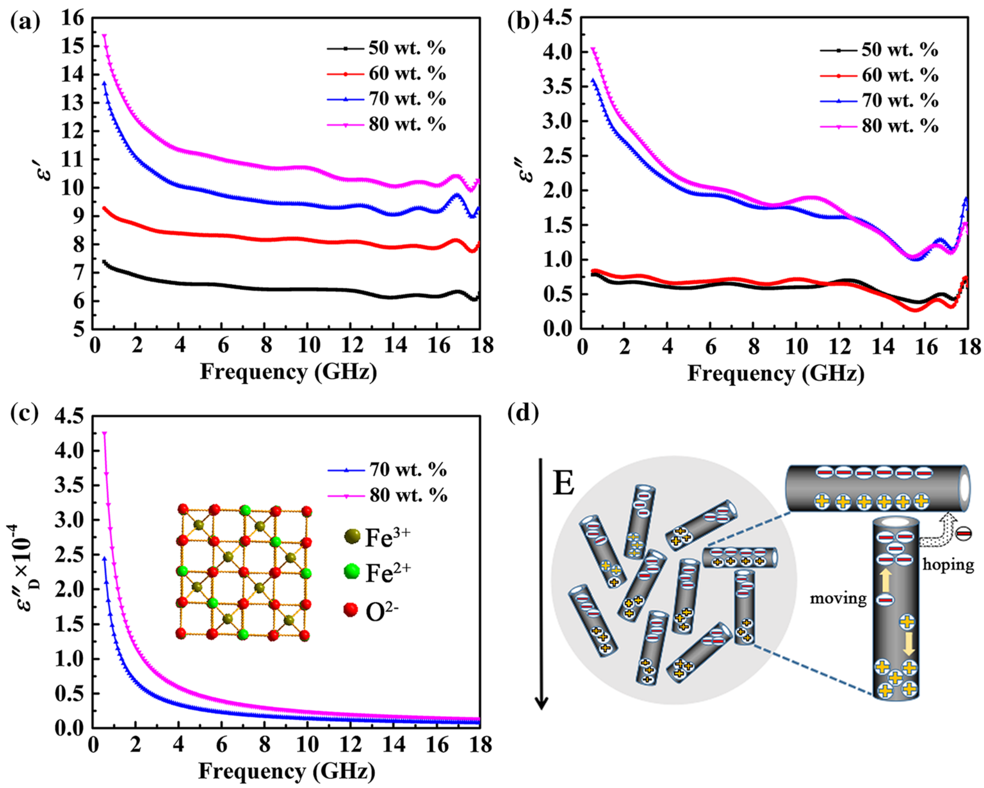

Figure 5 Frequency dependence of **a** real, **b** imaginary parts of complex permittivity, **c** direct current conduction loss for Fe_3O_4 nanotubes composite. *Inset* is the crystal structure of Fe_3O_4. **d** Schematic diagram of dielectric loss mechanism.

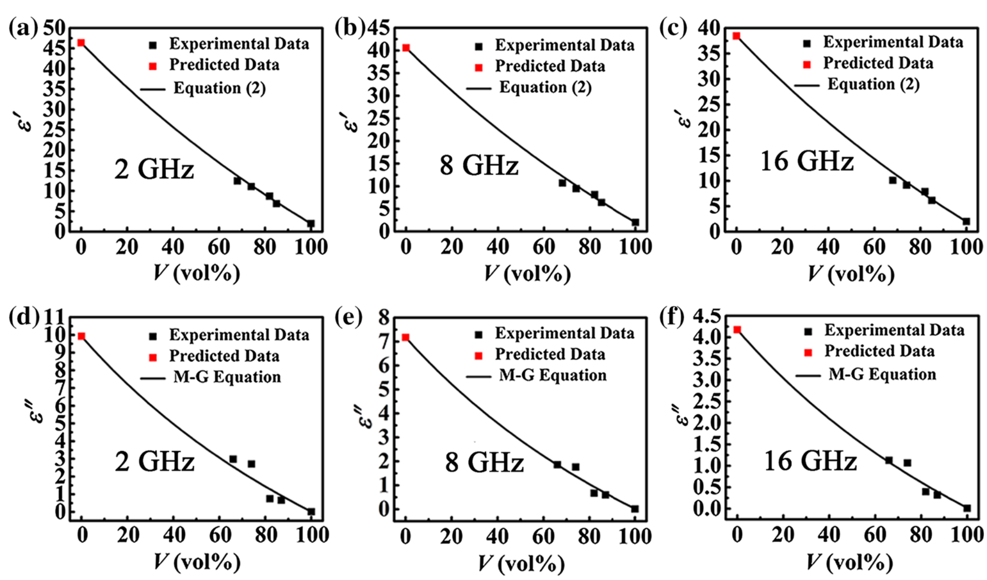

Figure 6 Concentration dependence of **a**–**c** ε', **d**–**f** ε'' for Fe_3O_4 nanotubes composites at various frequencies.

gets larger. Therefore, the two samples with 50 and 60 wt% cannot be measured for γ. Electronic relaxation polarization is depicted as the weakly bound electrons moving along the direction of the electric field in the surface of Fe_3O_4 nanotubes. For the electronic displacement polarization, the displacement is about 10^{-14} m; then, the relaxation time is about 10^{-14}–10^{-15} s. According to the same method, the relaxation time for electronic relaxation is calculated to 10^{-7}–10^{-8} s considering that the

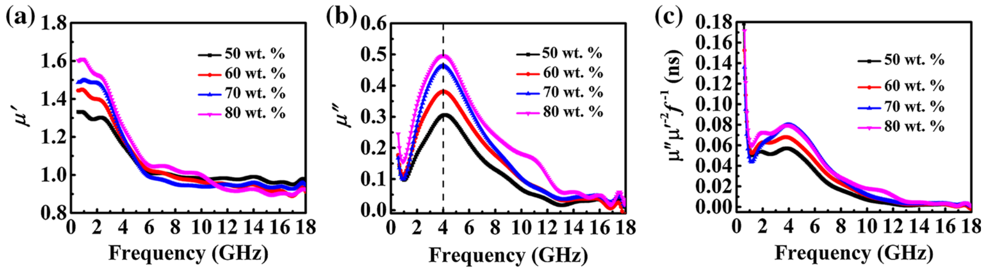

Figure 7 Frequency dependence of **a** real, **b** imaginary parts of complex permeability for Fe_3O_4 nanotubes composites. **c** Value of eddy current coefficient $\mu''\mu'^{-2}f^{-1}$ for the composites versus frequencies in the range of 0.5–18 GHz.

displacement of composite is the mean length of the nanotubes (10^{-7} m). Therefore, the corresponding resonance peak frequency is 1–10 MHz, which is the reason for the rapid decline of ε'' from 0.5 to 2 GHz.

Based on the effective dielectric theory, the relationship between effective permittivity of composite and permittivity of paraffin wax can be expressed by [31]

$$\frac{\varepsilon'_{eff} - \varepsilon'_F}{\varepsilon'_{eff} + 3\varepsilon'_F} = V\frac{\varepsilon'_W - \varepsilon'_F}{\varepsilon'_W + 3\varepsilon'_F} \quad (2)$$

where V is volume fraction of paraffin wax, ε_{eff}' is the effective permittivity of composites, ε_W' is permittivity of paraffin wax ($\varepsilon_W' = 2$), and ε_F' is permittivity of pure Fe_3O_4 nanotubes, which is smaller than that of corresponding bulk Fe_3O_4 due to the existence of atmosphere located in nanotubes. The theoretical results are in agreement with the experimental data as shown in Fig. 6a–c. On the other hand, ε'' can be well described by the Maxwell–Garnett model, which is shown in Fig. 6d–f [32]. The predicated intrinsic ε' of pure Fe_3O_4 nanotubes is around 46.4, 40.6 and 38.5 at 2, 8 and 16 GHz, respectively. And the predicated intrinsic ε'' is about 9.8, 7.2 and 4.2 at 2, 8 and 16 GHz, respectively. It is observed that the data distributions in Fig. 6 are similar at different GHz. The reason is that the size of ferroferric oxide nanotubes is much less than the wavelength at GHz and no relaxation resonance peak exists in the investigated frequency range.

Figure 7a, b represents the real and imaginary parts of the complex permeability (μ', μ''). From 0.5 to 6 GHz, the μ' for each sample significantly decreases with increasing frequency, and above 6 GHz, the μ' for each sample keeps constant, which is caused by the Snoeks' limit [33]. In addition, the μ'' value for each sample exhibits a strong peak at 4 GHz. In order to understand the unique behavior of the μ'', the value of eddy current coefficient

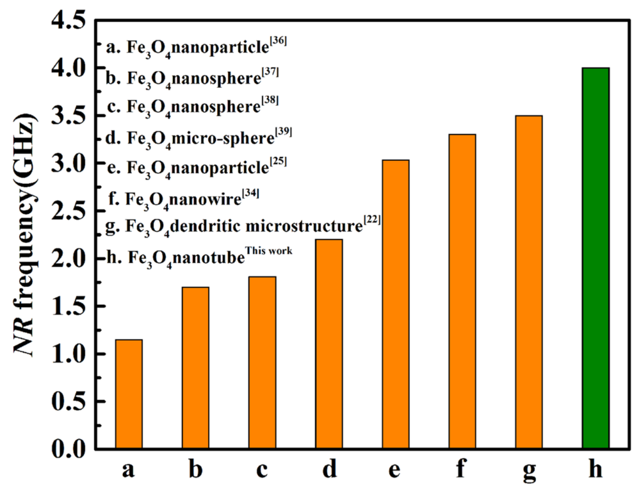

Figure 8 The natural resonance frequency for various Fe_3O_4 nanostructure.

$\mu''\mu'^{-2}f^{-1}$ is calculated. In general, the microwave magnetic loss originates chiefly from hysteresis, natural ferromagnetic resonance, domain wall resonance and micro-eddy current loss. Hysteresis losses are those that occur even at DC or low frequencies, and the domain wall resonance occurs usually less than 0.1 GHz. Besides, if the magnetic loss is mainly contributed by eddy current loss, the eddy current coefficient $\mu''(\mu')^{-2}f^{-1}$ should be almost constant at different frequencies. As shown in Fig. 7c, the eddy current loss could also be excluded due to the large difference in eddy current coefficients. Thus, the microwave magnetic loss attributes to natural ferromagnetic resonance. And the natural resonance (NR) frequency (4 GHz) is higher than that of bulk Fe_3O_4 (1.2 GHz), which is caused by the increase in the shape anisotropy [34, 35]. Such shift is larger than other that of Fe_3O_4 nanostructures (Fig. 8), and it can profoundly improve the microwave absorption due to the higher magnetic loss in the radar band (2–18 GHz).

To investigate the microwave absorbing properties, the reflection loss (RL) can be calculated from the relative complex permittivity and permeability according to the following equation [36]:

$$\mathrm{RL(dB)} = 20\log\left|\frac{Z_{in}-1}{Z_{in}+1}\right| \tag{3}$$

$$Z_{in} = \sqrt{\frac{\mu_r}{\varepsilon_r}}\tanh\left[j\left(\frac{2f\pi d}{c}\right)\sqrt{\mu_r\varepsilon_r}\right] \tag{4}$$

where ε_r and μ_r are the relative complex permittivity and permeability of the composite medium, respectively, Z_{in} is the normalized input impedance, c is the velocity of electromagnetic waves in vacuum, d is the thickness of the absorber.

Figure 9 shows the frequency dependence of reflection loss and d/λ_D (d is thickness, λ_D is the wavelength in dielectrics) for all samples at different thickness. The samples with 70 and 80 wt% show good microwave absorbing properties, while the 50 and 60 wt% microwave absorption are poor, which may be caused by the low dielectric loss (Fig. 5b). As exhibited in Fig. 9c, d, g, h, the absorption peaks are in the neighboring positions of $d/\lambda_D = (2k+1)/4$ (where k is a positive integer), suggesting that the reflection loss is caused by quarter-wavelength resonance. Therefore, the reflection peak shifted to lower frequencies with the increase in thickness. In

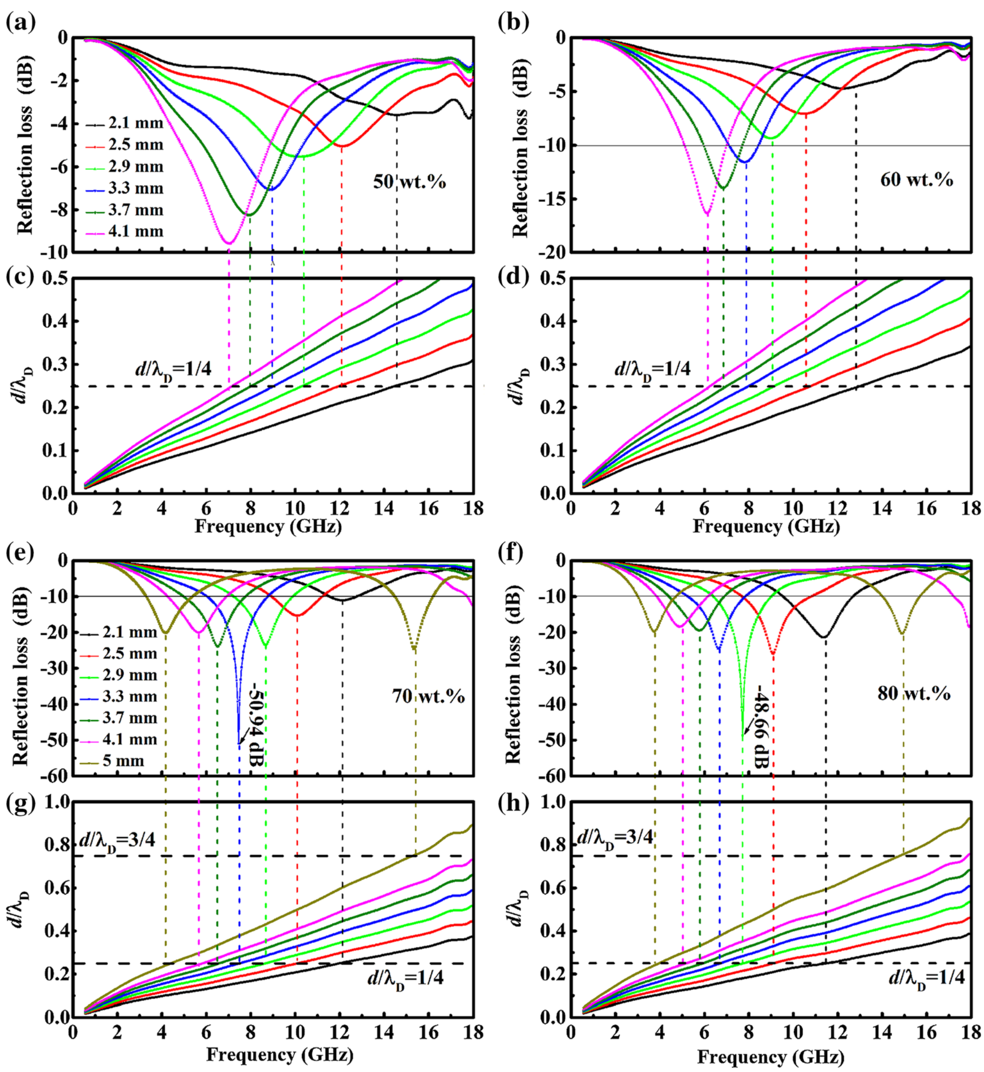

Figure 9 Reflection loss of composite with different Fe_3O_4 nanotubes weight fraction (**a**, **b**, **e**, **f**) for different layer thickness. The frequency dependence of d/λ_D for different Fe_3O_4 nanotubes weight fraction (**c**, **d**, **g**, **h**).

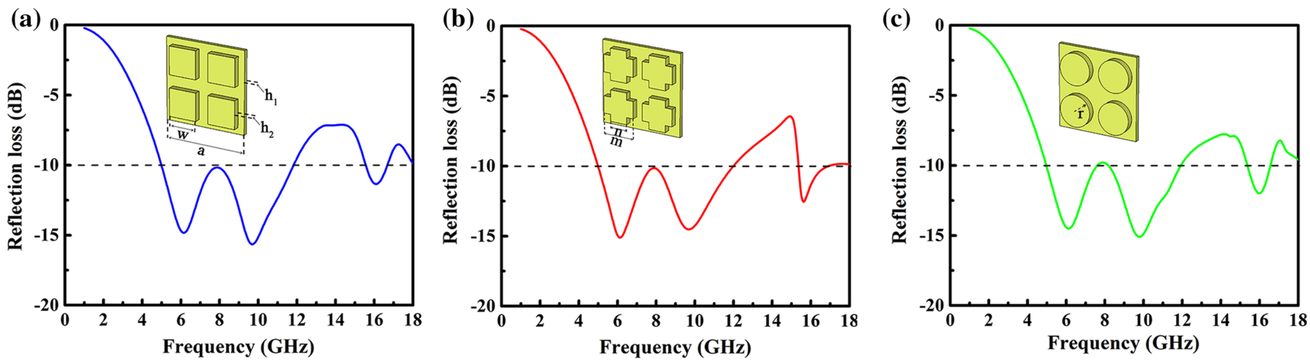

Figure 10 Reflection loss of Fe_3O_4 nanotubes metastructure with three kinds of patterns, **a** square, **b** cross, **c** circle, and corresponding parameters are show in the *insets*. Here, $h_1 = 2.1$, $h_2 = 2.9$, $W = 13$, $a = 38$, $n = 8$, $m = 14$ and $r = 7.3$ mm.

addition, double loss peaks can be observed in 70 and 80 wt% with thickness 5 mm. The first peak just meets the condition for $d/\lambda_D = 1/4$, and the second peak just meets the condition for $d/\lambda_D = 3/4$. Such microwave absorbing properties play an important role in designing broadband absorption metastructure. By using the electromagnetic properties of the sample with 80 wt%, three metastructures are designed. In the metastructures, the absorption band can be broadened by combating multiple resonances at different thickness (2.1 and 5.0 mm) [37]. As shown in Fig. 10, there are three absorption peaks in all metastructures, which significantly broaden the absorption bandwidth. The three absorption peaks resulted from the coupling of $\lambda/4$ resonance at 2.1 mm, $\lambda/4$ and $3\lambda/4$ resonances at 5.0 mm. The two absorption peaks at low frequency (around 6 and 10 GHz) are produced by the overlap of absorption peaks at 3.67 and 11.32 GHz corresponding to 2.1 and 5 mm, respectively. The third absorption peak at about 16 GHz is caused by the shift of $3\lambda/4$ resonances at 5.0 mm due to pattern structure. Each metastructure shows almost similar reflection loss except the little difference from 14 to 18 GHz resulted from the different edge scattering [37]. Strong absorption peaks of Fe_3O_4 nanotubes at various thicknesses are essential to broaden the absorption bandwidth by using the metastructure design.

For Fe_3O_4 nanotubes with 70 wt%, the bandwidth (RL < -10) is 2.75 GHz (Fig. 9), which is better than other Fe_3O_4 nanostructure with similar concentration, such as Fe_3O_4 nanospheres [38] and Fe_3O_4 hollow microspheres [39]. Meanwhile, Fe_3O_4 hollow microspheres also exhibit broadened absorption bandwidth, suggesting that hollow structure has the superiority of microwave absorption. Moreover, the microwave absorption of Fe_3O_4 nanotube could be further improved by filling other materials to improve heterogeneous interface polarization. Such strategy has been reported in carbon nanotube. For example, Qiu et al. [40] reported that magnetite nanoparticle–carbon nanotube–hollow carbon fiber composites (Fe_3O_4–CNTs–HPCFs) possessed the better electromagnetic wave absorbing performances than CNTs–HPCFs. Lu et al. [41] prepared Fe_3O_4 nanopearl decorated carbon nanotubes stemming from carbons onions (CNOs/CNTs@Fe_3O_4), which exhibited better microwave absorbing properties compared with CNOs/CNTs. However, holding the coexistence of various relaxations to improve the absorption bandwidth is still a challenging work.

Conclusions

In summary, Fe_3O_4 nanotubes were obtained through two-step chemical methods. The complex permittivity, complex permeability, microwave absorption and magnetic properties of the Fe_3O_4 nanotubes were investigated. Compared with other Fe_3O_4 nanostructure, Fe_3O_4 nanotubes show broader absorption bandwidth. The minimum RL reaches −50.94 dB at 7.45 GHz, and the absorption bandwidth below −10 dB reaches 2.75 GHz for Fe_3O_4 nanotubes composite with 70 wt%. What is more, both 70 and 80 wt% samples possess double loss peaks at 5 mm thickness. A metastructure absorber with better performance based on sample of the 80 wt% is designed, and the designed absorber possesses three absorption peak and 8 GHz bandwidth (RL < -10 dB). Thus, broad and significant applications of Fe_3O_4

nanotubes in microwave absorption and other fields may be envisaged.

Acknowledgements

This research was supported by the National Natural Science Foundation of China (Grant No. 51302312), BUCT Fund for Disciplines Construction (Project No. XK1702), and the Fundamental Research Funds for the Central Universities (Jd1601).

Compliance with ethical standards

Conflict of interest The authors declare that they have no conflict of interest.

References

[1] Balci O, Polat EO, Kakenov N, Kocabas C (2015) Graphene-enabled electrically switchable radar-absorbing surfaces. Nat Commun 6:6628

[2] Sun H, Che RC, You X, Jiang YS, Yang ZB, Deng J, Qiu LB, Peng HS (2014) Cross-stacking aligned carbon-nanotube films to tune microwave absorption frequencies and increase absorption intensities. Adv Mater 26:8120–8125

[3] Cao MS, Yang J, Song WL, Zhang DQ, Wen B, Jin HB, Hou ZL, Yuan J (2012) Ferroferric oxide/multiwalled carbon nanotube vs. polyaniline/ferroferric oxide/multiwalled carbon nanotube multiheterostructures for highly effective microwave absorption. ACS Appl Mater Interfaces 4:6948–6955

[4] Song WL, Guan XT, Fan LZ, Zhao YB, Cao WQ, Wang CY, Cao MS (2016) Strong and thermostable polymeric graphene/silica textile for lightweight practical microwave absorption composites. Carbon 100:109–117

[5] Kong L, Yin XW, Zhang YJ, Yuan XY, Li Q, Ye F, Cheng LF, Zhang LT (2013) electromagnetic wave absorption properties of reduced graphene oxide modified by maghemite colloidal nanoparticle clusters. J Phys Chem C 117:19701–19711

[6] Li Y, Cao WQ, Yuan J, Wang DW, Cao MS (2015) Nd doping of bismuth ferrite to tune electromagnetic properties and increase microwave absorption by magnetic–dielectric synergy. J Mater Chem C 3:9276–9282

[7] Saini P, Choudhary V, Singh BP, Mathur R-B, Dhawan SK (2009) Polyaniline–MWCNT nanocomposites for microwave absorption and EMI shielding. Mater Chem Phys 113:919–926

[8] Zhou W, Hu X, Bai X, Zhou S, Sun C, Yan J, Chen P (2011) Synthesis and electromagnetic, microwave absorbing properties of core-shell Fe_3O_4-poly (3,4-ethylenedioxythiophene) microspheres. ACS Appl Mater Interfaces 3:3839–3845

[9] Ting TH, Yu RP, Jau YN (2011) Synthesis and microwave absorption characteristics of polyaniline/NiZn ferrite composites in 2–40 GHz. Mater Chem Phys 126:364–368

[10] He P, Hou ZL, Wang CY, Li ZJ, Jing J, Bi S (2017) Mutual promotion effect of Pr and Mg co-substitution on structure and multiferroic properties of $BiFeO_3$ ceramic. Ceram Int 43:262–267

[11] Lee CC, Yoshikawa N, Taniguchi S (2011) Microwave-induced substitutional-combustion reaction of Fe_3O_4/Al ceramic matrix porous composite. J Mater Sci 46:7004–7011. doi:10.1007/s10853-011-5669-3

[12] He S, Wang GS, Wang JW, Wei YZ, Wu Y, Guo L, Cao MS (2013) Facile size-controllable synthesis of colorful quasi-cubic-Fe_2O_3 materials from nanoscale to microscale and their properties related to the size effect. ChemPlusChem 78:875–883

[13] Chen H, Wei W, Liu J, Fang D (2012) Propagation of a mode-Ill interfacial crack in a piezoelectric-piezomagnetic bi-material. Int J Solids Struct 49:2547–2558

[14] Zhou H, Zhang H, Pei Y, Chen HS, Zhao H, Fang D (2015) Scaling relationship among indentation properties of electromagnetic materials at micro- and nanoscale. Appl Phys Lett 106:081904

[15] Qu B, Zhu CL, Li CY, Zhang XT, Chen YJ (2016) Coupling hollow Fe_3O_4–Fe nanoparticles with graphene sheets for high-performance electromagnetic wave absorbing material. ACS Appl Mater Interfaces 8:3730–3735

[16] Chen HS, Wang HL, Pei YM, Wei YJ, Liu B, Fang DN (2015) Crack instability of ferroelectric solids under alternative electric loading. J Mech Phys Solids 81:75–90

[17] Pan YF, Wang GS, Yue YH (2015) Fabrication of Fe_3O_4@SiO_2@RGO nanocomposites and their excellent absorption properties with low filler content. Rsc Adv 5:71718–71723

[18] Shen X, Song F, Xiang J, Liu M, Zhu Y, Wang Y (2012) Shape anisotropy, exchange-coupling interaction and microwave absorption of hard/soft nanocomposite ferrite microfibers. J Am Ceram Soc 95:3863–3870

[19] Wang G, Gao Z, Tang S, Chen C, Duan F, Zhao S, Lin S, Feng Y, Zhou L, Qin Y (2012) Microwave absorption properties of carbon nanocoils coated with highly controlled magnetic materials by atomic layer deposition. ACS Nano 6:11009–11017

[20] Zhu H, Zhang H, Chen Y, Li Z, Zhang D, Zeng G, Huang Y, Wang W, Wu Q, Zhi C (2016) The electromagnetic property and microwave absorption of wormhole-like mesoporous carbons with different surface areas. Mater Sci 51:9723–9731

[21] Chen YJ, Zhang AB, Ding LC, Liu Y, Lu HL (2016) A three-dimensional absorber hybrid with polar oxygen functional groups of MWNTs/graphene with enhanced microwave absorbing properties. Compos Part B-Eng 108: 386–392

[22] Sun G, Dong B, Cao M, Wei B, Hu C (2011) Hierarchical dendrite-like magnetic materials of Fe_3O_4, γ-Fe_2O_3, and Fe with high performance of microwave absorption. Chem Mater 23:1587–1593

[23] Li ZJ, Hou ZL, Song WL, Liu XD, Cao WQ, Shao XH, Cao MS (2016) Unusual continuous dual absorption peaks in Ca-doped $BiFeO_3$ nanostructures for broadened microwave absorption. Nanoscale 8:10415–10424

[24] Liu Y, Cui T, Wu T, Li Y, Tong G (2016) Excellent microwave-absorbing properties of elliptical Fe_3O_4 nanorings made by a rapid microwave-assisted hydrothermal approach. Nanotechnology 27:165707

[25] Wen F, Zhang F, Zheng H (2012) Microwave dielectric and magnetic properties of superparamagnetic 8-nm Fe_3O_4 nanoparticles. J Magn Magn Mater 324:2471–2475

[26] Zhu YF, Fu YQ, Natsuki T, Ni QQ (2013) Fabrication and microwave absorption properties of $BaTiO_3$ nanotube/polyaniline hybrid nanomaterials. Polym Compos 34:265–273

[27] Qi X, Xu J, Hu Q, Deng Y, Xie R, Jiang Y, Zhong W, Du Y (2016) Metal-free carbon nanotubes: synthesis, and enhanced intrinsic microwave absorption properties. Sci Rep 6:28310

[28] Wang H, Wan L, Zhang J, Chen Y, Hu W, Liu L, Zhong C, Deng Y (2016) Enhanced microwave absorbing properties of surface-modified Co–Ni–P nanotubes. Mater Lett 169:193–196

[29] Hou ZL, Zhang M, Kong LB, Fang HM, Li ZJ, Zhou HF, Jin HB, Cao MS (2013) Microwave permittivity and permeability experiments in high-loss dielectrics: caution with implicit Fabry–Perot resonance for negative imaginary permeability. Appl Phys Lett 103:162905

[30] Torres-Heredia JJ, López-Urías F, Muñoz-Sandoval E (2005) Micromagnetic simulation of iron nanorings. J Magn Magn Mater 294:e1–e5

[31] Liu XD, Hou ZL, Zhang BX, Zhan KT, He P, Zhang KL, Song WL (2016) A general model of dielectric constant for porous materials. Appl Phys Lett 108:102902

[32] Jaouen V, Brayner R, Lantiat D, Steunou N, Coradin T (2010) In situ growth of gold colloids within alginate films. Nanotechnology 21:185605

[33] Li X, Han X, Tan Y, Xu P (2008) Preparation and microwave absorption properties of Ni–B alloy-coated Fe_3O_4 particles. J Alloys Compd 464:352–356

[34] Han R, Li W, Pan W, Zhu M, Zhou D, Li F (2014) 1D magnetic materials of Fe_3O_4 and Fe with high performance of microwave absorption fabricated by electrospinning method. Sci Rep 4:7493

[35] Liu Q, Zi Z, Zhang M, Zhang P, Pang A, Dai J, Sun Y (2013) Solvothermal synthesis of hollow glass microspheres/Fe_3O_4 composites as a light weight microwave absorber. J Mater Sci 48:6048–6055. doi:10.1007/s10853-013-7401-y

[36] Ni S, Lin S, Pan Q, Yang F, Huang K, He D (2009) Hydrothermal synthesis and microwave absorption properties of Fe_3O_4 nanocrystals. J Phys D Appl Phys 42:055004

[37] Li W, Wu T, Wang W, Zhai P, Guan J (2014) Broadband patterned magnetic microwave absorber. J Appl Phys 116:044110

[38] Jia K, Zhao R, Zhong J, Liu X (2010) Preparation and microwave absorption properties of loose nanoscale Fe_3O_4 spheres. J Magn Magn Mater 322:2167–2171

[39] Xu HL, Shen Y, Bi H, Liang WF, Yang R (2012) Preparation and microwave absorption properties of Fe_3O_4 hollow microspheres. Ferroelectrics 435:98–103

[40] Qiu J, Qiu T (2015) Fabrication and microwave absorption properties of magnetite nanoparticle-carbon nanotube–hollow carbon fiber composites. Carbon 81:20–28

[41] Lu X, Wu Y, Cai H, Qu X, Ni L, Teng C, Zhu Y, Jiang L (2015) Fe_3O_4 nanopearl decorated carbon nanotubes stemming from carbon onions with self-cleaning and microwave absorption properties. Rsc Adv 5:54175–54181